



**HAL**  
open science

## Authoring and Simulating Meandering Rivers

Axel Paris, Eric Guérin, Pauline Collon, Eric Galin

► **To cite this version:**

Axel Paris, Eric Guérin, Pauline Collon, Eric Galin. Authoring and Simulating Meandering Rivers. ACM Transactions on Graphics, In press, 42 (6), pp.14. 10.1145/3618350 . hal-04227965

**HAL Id: hal-04227965**

**<https://hal.science/hal-04227965v1>**

Submitted on 4 Oct 2023

**HAL** is a multi-disciplinary open access archive for the deposit and dissemination of scientific research documents, whether they are published or not. The documents may come from teaching and research institutions in France or abroad, or from public or private research centers.

L'archive ouverte pluridisciplinaire **HAL**, est destinée au dépôt et à la diffusion de documents scientifiques de niveau recherche, publiés ou non, émanant des établissements d'enseignement et de recherche français ou étrangers, des laboratoires publics ou privés.

# Authoring and Simulating Meandering Rivers

AXEL PARIS, Adobe Research, Université de Lyon, LIRIS, CNRS, UMR5205, France

ERIC GUÉRIN, Université de Lyon, LIRIS, CNRS, UMR5205, France

PAULINE COLLON, Université de Lorraine, GeoRessources, CNRS, F-54000 Nancy, France

ERIC GALIN, Université de Lyon, LIRIS, CNRS, UMR5205, France

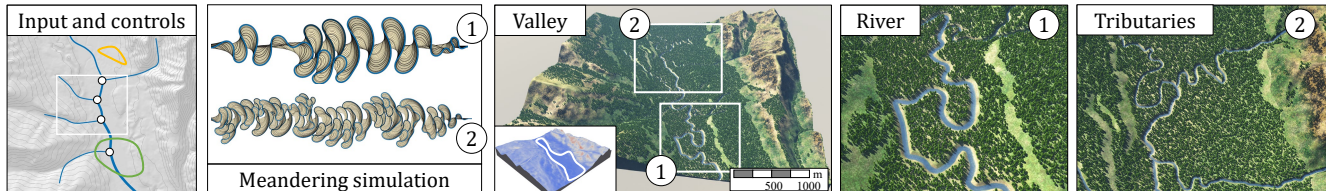


Fig. 1. Our method simulates a migrated meandering river network using a vector-based data structure. The migration models conform to the topography and dampens migration according to the slope or user-prescribed constraints. We record the evolution of the river network, approximate the erosion and sediment deposition processes to produce a vegetation density map, and augment the terrain with oxbow lakes filled with sediments and vegetation.

We present a method for interactively authoring and simulating meandering river networks. Starting from a terrain with an initial low-resolution network encoded as a directed graph, we simulate the evolution of the path of the different river channels using a physically-based migration equation augmented with control terms. The curvature-based terms in the equation allow us to reproduce phenomena identified in geomorphology, such as downstream migration of bends. Control terms account for the influence of the landscape topography and user-defined river trajectory constraints. Our model implements abrupt events that shape meandering networks, such as cutoffs forming oxbow lakes and avulsions. We visually show the effectiveness of our method and compare the generated networks quantitatively to river data by analyzing sinuosity and wavelength metrics. Our vector-based model runs at interactive rates, allowing for efficient authoring of large-scale meandering networks.

CCS Concepts: • **Computing methodologies** → **Shape modeling**.

Additional Key Words and Phrases: Erosion Simulation, Rivers, Procedural Generation

## ACM Reference Format:

Axel Paris, Eric Guérin, Pauline Collon, and Eric Galin. 2023. Authoring and Simulating Meandering Rivers. *ACM Trans. Graph.* 42, 6, Article 241 (March 2023), 14 pages. [https://doi.org/0000001.0000001\\_2](https://doi.org/0000001.0000001_2)

## 1 INTRODUCTION

The effective authoring of realistic and hydrologically consistent synthetic terrains is an open problem for many reasons. The challenge stems not only from the complexity of the underlying natural phenomena that shape the terrain, but also from the design of authoring tools that should provide a balance between physical accuracy

Authors' addresses: Axel Paris, Adobe Research, Université de Lyon, LIRIS, CNRS, UMR5205, France, [axel.paris@liris.cnrs.fr](mailto:axel.paris@liris.cnrs.fr); Eric Guérin, Université de Lyon, LIRIS, CNRS, UMR5205, France, [eric.guerin@liris.cnrs.fr](mailto:eric.guerin@liris.cnrs.fr); Pauline Collon, Université de Lorraine, GeoRessources, CNRS, F-54000 Nancy, France, [pauline.collon@univ-lorraine.fr](mailto:pauline.collon@univ-lorraine.fr); Eric Galin, Université de Lyon, LIRIS, CNRS, UMR5205, France, [eric.galin@liris.cnrs.fr](mailto:eric.galin@liris.cnrs.fr).

© 2023 Association for Computing Machinery.

This is the author's version of the work. It is posted here for your personal use. Not for redistribution. The definitive Version of Record was published in *ACM Transactions on Graphics*, [https://doi.org/0000001.0000001\\_2](https://doi.org/0000001.0000001_2).

and precise user control while allowing for interactive feedback during editing.

Existing techniques frequently focus on mountainous landforms such as large-scale dendritic mountain ranges, mesoscale canyons and glacier valleys featuring moraines and screes, and small-scale erosion landmarks such as ravines. In contrast, generating plains with the complicated and diversified shapes of meandering river networks together with their associated landscapes received less attention in Computer Graphics, even though they play a crucial part in the overall visual aspect.

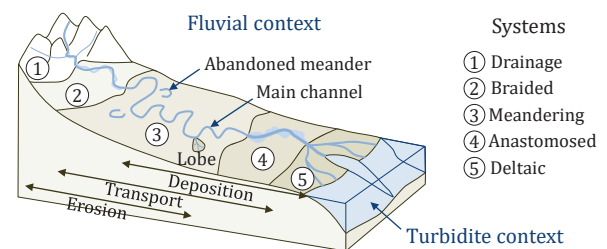


Fig. 2. Background on the geomorphology of rivers: meandering systems are found mostly in regions where the slope is small.

Rivers (also referred to as *channels*) organize themselves in various networks depending on their geographical locations (Figure 2): from confined, small torrential streams in mountains, they form braided systems before evolving to single, meandering and potentially large rivers in the alluvial plains.

Anastomosed systems were often presented as a braided morphology observed also in plains. [Makaske 2001] clarified this, by defining them as *composed of two or more interconnected channels that enclose floodbasins*. Thus, floodplains can also develop locally braided systems, depending on the combined effects of flow discharge, sediment load, avulsion rate, and local slope. In this work, we focus only on meandering systems. Those are characterized by their dynamic: erosion on the river outer bank occurs together

with deposition on the inner bank, leading to a progressive lateral migration of the channel [Huggett 2003].

Simulating realistic and hydrologically-consistent river networks is a demanding task. Existing techniques [Génevaux et al. 2013; Kelley et al. 1988; Peytavie et al. 2019] first compute a low-resolution river network before carving the riverbed into the bedrock and finally generate a plausible animated water surface according to the underlying relief of the riverbed. However, the resulting rivers are generated as static elements: their evolution through time and the strong impact on the surrounding landscape is neglected. The challenge stems from the fact that meandering channels are highly dynamic objects that migrate gradually, but also abruptly due to avulsions and cutoffs [Slingerland and Smith 2004; Stouthamer and Berendsen 2001]. The lateral migration rates can cover a wide range of values, up to several meters per year [Black et al. 2010] depending on various contextual parameters such as the sedimentary charge in the river, water discharge, climatic conditions, or vegetation. These complex, intricate parameters produce sinuous irregular trajectory patterns. In reaction, the surrounding landscape (topography, vegetation) is directly impacted by this migration.

Here, we introduce a new simulation method to reproduce the large-scale meandering behavior of rivers. We employ a physically-based approach to deform the trajectories of the different channels, accounting for environment parameters such as the local slope, upstream water discharge, and user-defined constraints. We replicate observed phenomena such as complex bend development, oxbow lake formation due to cutoffs, avulsion events, sediment deposition, and vegetation growth along the banks leading to landscapes featuring realistic river trajectories.

More precisely, the contributions of this paper include: 1) A method for simultaneously simulating and authoring the evolution of a meandering river through time using a curvature-based migration approach and allowing control over the simulation using a range of authoring tools (Section 4); 2) A framework for simulating abrupt events such as cutoffs and avulsions that dramatically change the channel paths, and also providing additional control to the designer (Section 5); 3) A global river network data structure, encoded as a directed graph of channels, adapted to compute collisions between the time-evolving channels (Section 6).

We bridge the gap between simulation and authoring by augmenting the channel migration equation with terms implementing attractive and repulsive regions for controlling the simulation, and for prescribing the trajectory of some parts of the different channels. Moreover, the recording of data during the simulation allows for computing some abiotic parameters, performing local terrain amplification and river bed carving, and generating vegetation (Section 7). Our method is compatible with other state-of-the-art terrain modeling techniques, operates interactively, and can be integrated into a production pipeline.

## 2 RELATED WORK

Here we review erosion simulation methods applied to river synthesis and focus on approaches addressing the creation of river networks. We refer the reader to [Galín et al. 2019] for a complete

review of terrain modeling techniques covering procedural generation, erosion simulation, and example-based synthesis. We also review related work in Geosciences aiming at reconstructing complete meandering channel complexes.

### 2.1 Methods from Computer Graphics

Some procedural generation approaches directly incorporate low resolution rivers in the terrain generation process. Kelley *et al.* [1988] first proposed a mid-point displacement algorithm to generate watersheds and river networks. Subdivision rules [Prusinkiewicz and Hammel 1993] and modified stochastic subdivision algorithms based on fractional Brownian motion [Belhadj and Audibert 2005] were proposed to refine the river paths. Hnaidi *et al.* [2010] proposed a general algorithm based on control curves for simultaneously manipulating rivers and ridge lines, and generating a terrain conforming to those constraints using a diffusion equation. This method was later extended by employing gradient space modeling [Guérin et al. 2022]. Génevaux *et al.* [2013] proposed a hydrologically-consistent terrain generation capable of producing large-scale river trajectories consistent with the Rosgen classification [Rosgen 1994]. Peytavie *et al.* [2019] presented an extension for generating static river trajectories and carving complex riverbed.

Procedural approaches mostly employ fractal spline curves as an approximation of the complex time-evolving patterns that can be observed and therefore fail to capture the complex shapes of channels, arising from a multi-factorial migration process. Moreover, they do not simulate their evolution throughout time.

Particle-based methods [Krištof et al. 2009; Skorkovská et al. 2019] and shallow water erosion [Beneš et al. 2006; Štava et al. 2008] reproduce ravines and gullies by simulating the transport and erosion of particles on the terrain, and can even yield meandering patterns and oxbows [Kurowski 2012] under the correct parameter setting. Limited in spatial scale, those methods do not lend themselves to reproducing large-scale meandering networks and only provide indirect control over the paths of rivers. Recent large-scale tectonic terrain generation techniques based on stream power erosion [Cordonnier et al. 2016; Schott et al. 2023] generate hydrologically-correct river networks. However, the time and spatial scale prevent those approaches from generating meandering river networks. Overall, existing erosion simulations do not lend themselves to controlling and generating meandering river networks.

We depart from existing procedural and erosion simulation approaches and present a controllable framework for simulating and authoring meandering river networks. Contrary to previously described techniques, we rely on a simulation of the evolution of the different channel trajectories using a physical model inspired by geomorphology allowing us to approximate moisture and sediment deposition, later used to generate plausible vegetation cover and sediments on the terrain.

### 2.2 Methods from Geosciences

Rivers have been studied for many years in Geosciences and various methods exist for their simulation. Here, we only review approaches that model the river as a discrete set of points, often denoted as the channel *centerline*, which are the most relevant to our method.

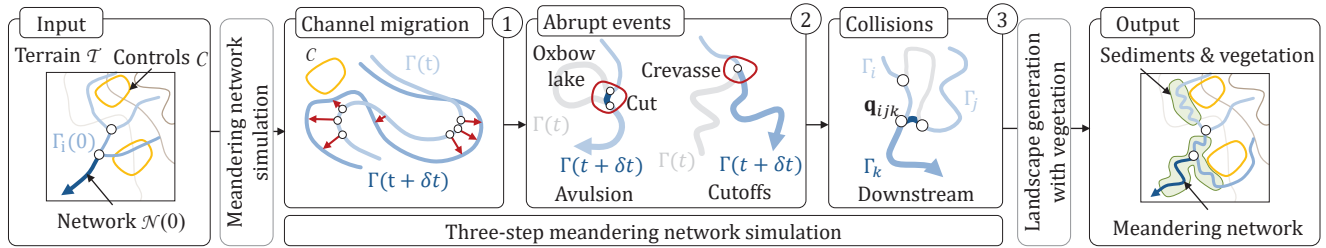


Fig. 3. Starting from an initial river network  $\mathcal{N}(0)$  automatically computed or provided by the user, the network simulation is performed on each channel  $\Gamma_j$ , and collisions between channels are finally resolved, leading to a network at time step  $\mathcal{N}(t + \delta t)$  exhibiting meandering patterns. Previous trajectories of all channels are recorded in the simulation data  $\mathcal{D} = \{\mathcal{N}(t)\}$ .

We refer the reader to [Brown and Pasternack 2019] for a complete overview of other techniques, and to geostatistical literature for cell-based methods.

Motivated by the need to perform accurate petroleum reservoir simulations, object-based methods were developed early to reconstruct complete 3D sedimentary records in fluvial environments [e.g., Clemetsen et al. 1990; Deutsch and Tran 2002; Viseur et al. 1998]. In this context of high uncertainties - past conditions are unknown and data are heterogeneous and sparse -, the methods are generally stochastic and generate independent single channels in the 3D volume to facilitate data conditioning [e.g., Bertonecello et al. 2013; Deutsch and Tran 2002; Deutsch and Wang 1996; Rongier et al. 2017b; Viseur et al. 1998]). To our knowledge, gradual migration has rarely been integrated into these works, or, for efficiency purposes, with geostatistical rules [e.g., Parquer et al. 2017; Rongier et al. 2017a]. Also, the proposed methods directly simulate sinuous centerlines without integrating topographical settings.

In parallel, process-based approaches have been developed to reproduce a geological history: from an initial location, and, if possible, topography and geological settings, these works integrate cutoff events, which are a key stabilization process in meandering systems, and avulsion, which is a sudden change of trajectory of the channel where the old path is completely abandoned. More recent works have focused on specific phenomena such as lateral or downstream bend migration [Posamentier and Kolla 2003], channel bend retro-migration [Nakajima et al. 2009], or avulsion [Pyrzcz et al. 2009]. Recent work from [Sylvester et al. 2019] analyzed the time-evolving behavior of real meanders using precise river elevation data. Their results suggest that lateral migration varies linearly with local and upstream curvature. Interested by generating the sedimentary pile, these algorithms generally integrate aggradation (or vertical migration), which moves the channel upward, even if, except for some vertical outcrops, most of the research on the river trajectory analyzes planar views from satellite or bathymetric data. However, aggradation changes the elevation of the terrain at large timescale, and can thus be neglected at the considered landscape and temporal scale. As the past topography and geological settings are rarely known with the required precision, the process-based methods mainly allow the geoscientists to test their hypotheses about the past settings and understand the geological history. The vegetation is generally not considered, and the user is not supposed to interfere during the simulation.

Existing works in Geosciences usually study the evolution of a single idealized channel throughout time. We present a method that overcome this limitation by enabling artists to author complex networks extending over plurikilometric terrains. Relying on the physically-based algorithm proposed by [Sylvester et al. 2019] for its computational efficiency, we augment it to simulate the evolution of the trajectory on each channel of the network, while accounting for the surrounding terrain as well as user-defined constraints.

### 3 OVERVIEW AND NOTATIONS

Our method computes the temporal evolution of a meandering river network over an input terrain  $\mathcal{T}$  under the combined action of migration forces due to curvature and slope and various events including avulsion and cutoffs (Figure 3). For the sake of computational efficiency and providing a real-time simulation compatible with authoring, we do not account for the influence of vegetation as reported in [Ielpi et al. 2022] and the incremental sediment deposition during the migration of meanders [Howard and Knutson 1984]. Instead, we record the evolution of the meandering network, which allows us to approximate the sediment deposition processes, which in turn, combined with the abiotic parameters derived from the channels, facilitates the generation of vegetation on the terrain.

#### 3.1 River network and channel models

The evolving river network  $\mathcal{N}(t)$  is a time-varying oriented geometric graph or tree, whose edges are channels  $\Gamma_i(t)$ , *i.e.* curves over the terrain  $\mathcal{T}$ , and whose nodes are static junction points  $\mathbf{q}_{ijk}$  connecting channels (Figure 4). The leaves of the tree represent the sources, and the root the outlet. In general, only two channels meet at a junction, therefore we represent  $\mathcal{N}(t)$  as a set of binary trees. Channels within the river graph are connected through junction points, referred to as  $\mathbf{q}_{ijk}$ , connecting two upstream channels  $\Gamma_i$  and  $\Gamma_j$  that meet and merge into a downstream channel  $\Gamma_k$  (see Figure 4).

At the heart of the simulation is the channel model, defined as a time-varying piecewise cubic spline curve  $\Gamma$  in the plane with  $n$  sampling points  $\{\mathbf{p}_k(t)\}$ ,  $k \in [0, n(t)[$ , evenly spaced at a distance

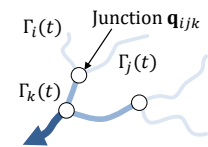


Fig. 4. Channels  $\Gamma_i(t)$  and junction points  $\mathbf{q}_{ijk}$ .

$\delta p$ . As meanders form in flat regions, a commonly used and valid approximation in Geosciences consists of performing computations in 2D at this stage. We denote  $\Gamma(t)$  the channel curve at time step  $t$ , and we refer to a point along the curve as  $\mathbf{p}(u, t)$ , with  $u \in [0, 1]$  the curvilinear abscissa (see Figure 5). Channel points have exactly one upstream and one downstream neighbor, except for the first and last points, which are connected to other channels in the network (see Section 6).

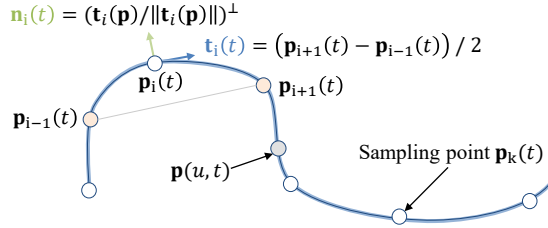


Fig. 5. A channel is defined as a set of equally-spaced sampling points  $\mathbf{p}_k(t)$  along the trajectory at a given time step  $t$ , with corresponding normals  $\mathbf{n}_k(t)$  and tangents  $\mathbf{t}_k(t)$ .

Channels are not only characterized by their sampling points  $\{\mathbf{p}_k(t)\}$ , but also by their flow  $\Phi_\Gamma$ , width  $w_\Gamma$  and depth  $d_\Gamma$  (Figure 6). Those parameters are computed according to power laws [Dunne 1978] that relate the drainage area to the width and depth of the channel. Let  $a$  denote the drainage area, the width of the channel is related to the drainage by the power law  $w_\Gamma \propto a^{0.5}$ . The width and depth of the river are then correlated by  $w_\Gamma = 18.8 d_\Gamma^{1.41}$  [Konsoer et al. 2013]. In our implementation, these values are constant for a given channel, a valid approximation often used in Geosciences and discussed in Section 8.5.

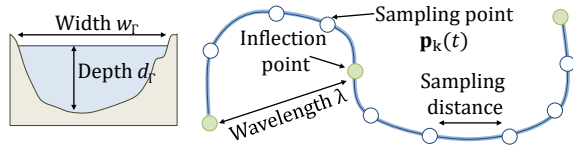


Fig. 6. A channel is characterized by its width  $w_\Gamma$  and its depth  $d_\Gamma$ . These are directly correlated to the wavelength  $\lambda$  of the meander bend, which is defined as the distance between two successive inflection points.

### 3.2 Workflow

Let  $\mathcal{T}$  define the initial input terrain, and  $h : \mathbb{R}^2 \rightarrow \mathbb{R}$  its elevation function. It may be either a discrete heightfield or a procedural representation [Galín et al. 2019]. The initial river network  $\mathcal{N}(0)$  may be either provided by the user or computed as described in [Peytavie et al. 2019]. In our framework, we first perform breaching on the terrain [Barnes et al. 2014] to remove unwanted pits (local minima), then compute the drainage area  $a$ , and finally select cells with a drainage value above a user-controlled threshold value to identify the cells that form the low-resolution river network.

The simulation computes a new network  $\mathcal{N}(t + \delta t)$  in three steps (Figure 3). We first compute channel migration, responsible for the

formation of meanders on each channel of the network (Section 4). Then, we simulate abrupt events such as cutoffs and avulsions (Section 5), which can drastically change the trajectories of the different channels. Finally, we resolve collisions that may occur between the migrated trajectories, and optionally place procedural river junctions patterns to better reproduce the various archetypes identified in Geomorphology (Section 6). Throughout the simulation, we record all channel trajectories leading to a simulation history  $\mathcal{D} = \{\mathcal{N}(t)\}$ . We can later use this history to procedurally compute abiotic parameters (Section 7) and place vegetation over the terrain.

## 4 CHANNEL SIMULATION

The simulation of the evolution of a given channel proceeds as follows. First, we compute *channel migration* (Section 4.1) which moves the sampling points  $\mathbf{p}_k$  of the channel laterally from the local and upstream curvature (Section 4.2) and resample the curve (Section 4.3) throughout time to guarantee stability. The channel migration (Section 4.1) is based on the model described by [Sylvester et al. 2019]: our contributions lie in the introduction of new terms to account for the topography of the terrain (Section 4.4) and the additional control provided to the user through control regions (Section 4.5).

Symbol	Value	Unit	Physical meaning
$\delta t$	106	d	Time step, Sylvester [2019]
$\omega$	-1	-	Migration weight, Howard [1984]
$\gamma$	2.5	-	Upstream weight, Howard [1984]
$k$	0.164	m/d	Migration speed, Sylvester [2019]
$f$	0.011	-	Friction factor, Sylvester [2019]
$\delta p$	50	m	Sampling distance
$s_0$	0.15	-	Slope threshold
$t_c$	0.1	-	Crevasse curvature threshold
$\rho_c$	0.05	[0, 1]	Crevasse probability
$\rho_a$	0.05	[0, 1]	Avulsion probability
$\alpha_0$	45	°	Avulsion initial angle
$\epsilon_a$	0.05	-	Avulsion slope threshold
$\epsilon_m$	[0, 1]	m/d	Moisture accumulation
$r_m$	$6w_\Gamma$	m	Radius of moisture
$\epsilon_s$	[0, 1]	m/d	Sediment accumulation
$r_s$	$4w_\Gamma$	m	Radius of sediment

Table 1. List of constants (upper rows) and simulation parameters (lower rows) with the corresponding notations, nominal values, and interpretation.

We report the values for the different parameters and constants of the simulation throughout the text and in Table 1. We emphasize the difference between constants taken from geomorphology and the parameters set by the user.

### 4.1 Channel migration

For a given channel  $\Gamma$ , the migration process computes new positions for the sampling points. Every point  $\mathbf{p}_k(t)$  at a given time step  $t$

migrates towards the direction of the normal to the channel  $\mathbf{n}_k(t)$ . Let  $\mathbf{t}_k(t) = \mathbf{p}'_k(t)$  denote the tangent of the curve and its unit version  $\hat{\mathbf{t}}_k(t) = \mathbf{t}_k(t)/\|\mathbf{t}_k(t)\|$ . We define the unit normal as the orthogonal vector oriented toward the sign of the local curvature  $\mathbf{n}_k(t) = \hat{\mathbf{t}}_k(t)^\perp$ . Let  $\delta t$  the time step, points then migrate according to their *migration rate*  $\mu$  following the equation:

$$\mathbf{p}_k(t + \delta t) = \mathbf{p}_k(t) + \mathbf{n}_k(t) \mu(\mathbf{p}_k(t)) \delta t \quad (1)$$

The time step  $\delta t$  is set to 106 days. Smaller values may not be relevant because of the migration speed of meanders, and larger values up to a year may be used safely without breaking the simulation. The challenge of Equation 1 stems from the computation of the migration rate  $\mu$ , which intuitively defines the movement speed through time. Howard and Knutson [1984] found that it can be directly correlated to the curvature of the river: high curvature sections, we describe the computation of the migration rate in geomorphology (Section 4.2) and the trajectory resampling process (Section 4.2), and then explain how we incorporate new terms to provide control to the user (Section 4.4 and Section 4.5).

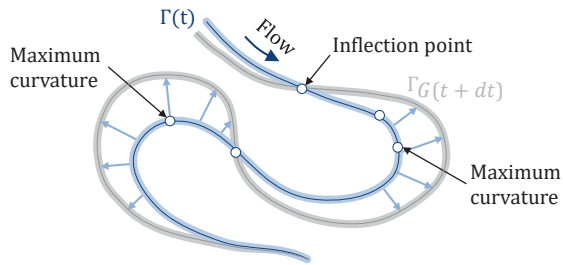


Fig. 7. Synthetic view of the channel migration using the simple migration rate  $\mu_0$ : the curve  $\Gamma(t)$  transforms into  $\Gamma_G(t + \delta t)$  and, in this case, the maximum migration point corresponds to the maximum curvature point.

Let  $x'$  and  $x''$  (respectively  $y'$  and  $y''$ ) denote the first and second derivatives along the  $x$  axis (respectively along the  $y$  axis) of the curve. The local curvature  $\phi_\Gamma(u, t)$  is defined as:

$$\phi_\Gamma(u, t) = \frac{x'(u, t) y''(u, t) - y'(u, t) x''(u, t)}{(x'(u, t)^2 + y'(u, t)^2)^{3/2}}$$

The channel is defined by a set of discrete points, thus derivatives are approximated using central differences. The *local migration rate*  $\mu_0$  is then defined by scaling the curvature according to the river width  $w_\Gamma$ , and  $k$  the local migration rate constant, set to 0.164m/day:

$$\mu_0(u, t) = w_\Gamma k \phi_\Gamma(u, t) \quad (2)$$

The value of  $k$  was set according to data for real river data (see Table 1). While this parameter could provide additional user control, we found it simpler to only disclose the timestep  $\delta t$  to the user and set the other coefficients as constants in the code. The linear scaling by the channel width  $w_\Gamma$  implies that the frequency of meander bends is proportional to the dimension of the river (width and depth), which has been identified and reported in multiple studies in Geomorphology [Leopold and Wolman 1960; Williams 1986]. Our simulation conforms to this observation, as demonstrated in

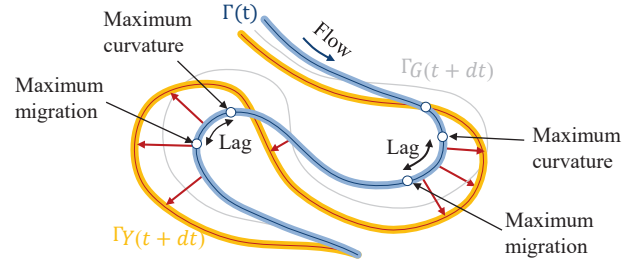


Fig. 9. The global migration rate  $\mu$  accounts for upstream curvature, which introduces a lag between the point of maximum curvature and the point of maximum migration.

Figure 10 where the wavelength of meander bends increases proportionally to the width of the channel.

Using the local migration rate model transforms the original curve  $\Gamma(t)$  into a new curve  $\Gamma_G(t + \delta t)$  with increased bends (see Figure 7, blue and grey curves). In this case, the maximum curvature point corresponds to the maximum migration point. Inflection points, *i.e.* such that  $\phi_\Gamma(u, t) = 0$ , correspond to the intersection points between  $\Gamma(t)$  and  $\Gamma(t + \delta t)$ . However, using only the local migration does not lead to realistic meandering patterns, as meanders are also influenced by upstream trajectories. Particularly, high curvature *upstream bends* tend to increase the migration rate [Howard and Knutson 1984].

## 4.2 Upstream curvature-based migration

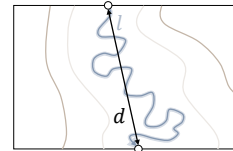


Fig. 8. Sinuosity.

Following the model proposed by Sylvester *et al.* [2019], we consider the influence of the upstream curvature to compute a more accurate *global migration rate*  $\mu$ . Let  $\sigma$  denote the sinuosity of the channel (Figure 8), which is computed as the ratio between the curvilinear length of the curve  $l$  and the distance between the first and the last points of the section:

$$\sigma = l / \|\mathbf{p}(0, t) - \mathbf{p}(1, t)\|, \quad l = \int_0^1 \|\nabla \mathbf{p}(\zeta, t)\| d\zeta \quad (3)$$

The global migration rate along the curve is finally defined from the combination of the local migration rate  $\mu_0$  and the integral of upstream migration rates:

$$\mu(u, t) = \omega \mu_0(u, t) + \sigma^{-2/3} \left[ \gamma \int_0^\infty \mu_0(u - \zeta, t) k(\zeta) d\zeta \right] \left[ \int_0^\infty k(\zeta) d\zeta \right]^{-1} \quad (4)$$

The variable  $\zeta$  denotes the upstream distance from the point  $\mathbf{p}(u, t)$ , and  $\omega$ ,  $\gamma$  are constant weighting parameters with values of  $-1$  and  $2.5$  that control the influence of local and upstream curvatures, respectively. As we found these difficult to control, we do not expose these parameters and rather provide control on the migration process through specific terms in the equations (see Section 4.5). Multiplying by  $\sigma$  implies that meanders with lots of bends migrate faster.

The kernel  $k$  is an exponentially decreasing weighting function:

$$k(\zeta) = e^{-\alpha\zeta} \quad (5)$$

The term  $\alpha$  is defined from a friction factor and the river depth  $d_\Gamma$  which is assumed to be uniform along the channel:  $\alpha = 2f/d_\Gamma$ . It defines a relation between the river depth  $d_\Gamma$  and the influence of upstream points: a point in a deeper river is influenced by points further away upstream. The friction constant  $f$  influences the size and amount of meander loops: low friction values lead to less meanders, while high values are correlated to high frequency, small meander loops. We set  $f$  to 0.011 to best reproduce the migration of real meandering rivers.

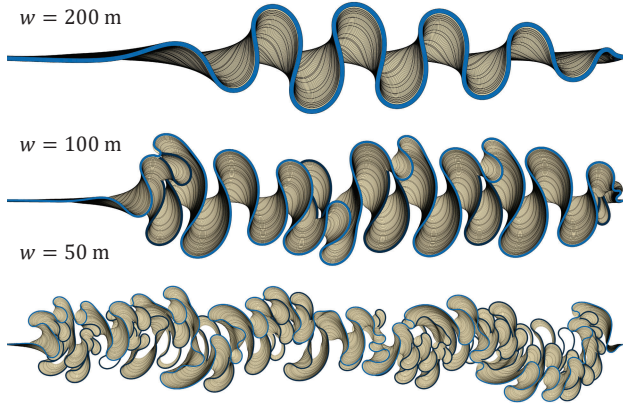


Fig. 10. Comparison between meandering rivers of different widths (100 years simulation): the wavelength  $\lambda$  is proportional to the river width  $w_\Gamma$ .

This definition of the global migration rate  $\mu$  in Equation 4 introduces a lag between the maximum curvature point and the maximum migration point, as emphasized by [Sylvester et al. 2019]. Figure 9 shows the channel  $\Gamma(t)$  (in blue) evolving into  $\Gamma_Y(t + \delta t)$  (in yellow), which significantly differs from the channel computed using the simple migration rate  $\Gamma_G(t + \delta t)$  (in grey). This formulation reproduces meander loops progressively moving downstream throughout time (Figure 11), a well-known phenomena called downstream migration.

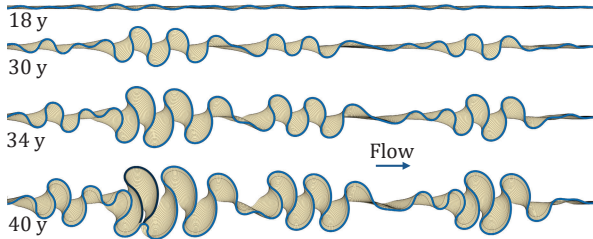


Fig. 11. Different steps of the meandering river simulation of a single channel. The latest trajectory is shaded in light blue, while older paths are shaded in brown. Upstream curvature impact meander bends that progressively migrate downstream.

### 4.3 Resampling

At every time step, the migration process (Section 4.1) moves the sampling points  $\mathbf{p}_j(t)$  laterally based on the local and upstream curvature. In practice, this leads to unevenly spaced points  $\mathbf{p}_j(t + \delta t)$ , which create instabilities after several simulation steps. To ensure stability, we apply a resampling step after the migration.

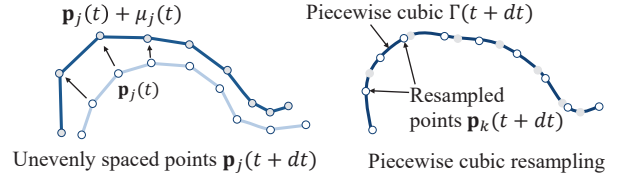


Fig. 12. After channel migration (Section 4.1), sampling points may be unevenly spaced, which is corrected by resampling the piecewise cubic curve  $\Gamma(t + \delta t)$  passing through the displaced sampling points.

We first compute the piecewise cubic spline curve  $\Gamma(t + \delta t)$  passing through the migrated sampling points  $\mathbf{p}_j(t + \delta t)$  along with their tangents  $\mathbf{t}(t + \delta t)$ . We then sample this curve at regular intervals  $\delta \mathbf{p}$ , and use these samples as the new sampling points of the channels  $\mathbf{p}_k(t + \delta t)$  (Figure 12). The sampling distance must respect the constraint  $\delta \mathbf{p} \leq w_\Gamma$  (we use  $\delta \mathbf{p} = 50$  m for all channels in our experiments). Note that the number of points of a given channel may change during resampling, but this is not a problem for the simulation. The only constraint is that the first and last points in the channel should be anchored and static, which is crucial for managing junctions as described in Section 6.1.

### 4.4 Terrain influence

Terrain topography has a strong influence on the development of meanders. In large plains, the channel is not constrained, which leads to complex meandering systems. Areas with a steep slopes prevent the development of meanders and create straight trajectories (transition zone), as reported by the Rosgen classification [Rosgen 1994]. In valleys, the channel may be meandering but remains constrained by the surrounding mountains (see Figure 13). In this section, we extend the migration equation from geomorphology to account for the influence of terrain topography on the migration process. While not mandatory in geomorphology, it is crucial in our context where artists aim at modeling river networks over large-scale complex terrains.

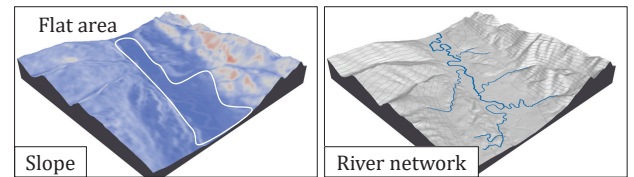


Fig. 13. Influence of the slope over the meandering process.

Recall that channel migration is defined by Equation 4, where  $\mu$  denotes the migration rate of the point. To model the terrain

influence, we define a modified rate  $\tilde{\mu}$  from the migration rate  $\mu$  (Equation 4), as a function of the local slope of the terrain  $s(\mathbf{p}) = \|\nabla h(\mathbf{p})\|$ :

$$\tilde{\mu}(u, t) = (g \circ s \circ \mathbf{p}(u, t)) \mu(u, t) \quad (6)$$

The falloff function  $g : \mathbb{R} \rightarrow [0, 1]$  is the smoothstep function, taking null value above a slope threshold  $s_0$  specified by the user. Figure 27 shows a three-stage meandering systems with meanders and oxbow lakes in plains, straight river trajectories due to steep slopes, and constrained meandering patterns in valleys surrounded by mountains. The user may modify the topography of the terrain interactively during the simulation and see the channels adapt automatically (see accompanying video).

#### 4.5 Controls

Combining the physically-based simulation of meandering river with user-control is a crucial feature of our approach, where we aim at preserving the overall realism of the meanders while allowing creativity for artists. We developed two different strategies: feature points and control regions. *Feature points* are a direct and straight-forward approach for controlling the trajectory. The user may move and lock the position of the sampling points  $\mathbf{p}_k$  or divide a given channel  $\Gamma_i$  into two connected sub channels. In contrast, *control regions* operate indirectly and either influence the direction of the migration, or dampen the migration rate, which is useful for handling junctions (see Section 6.1). These regions are defined through

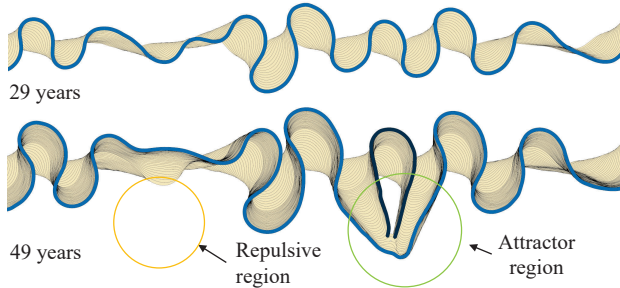


Fig. 14. Control regions allow the user to constrain the simulation without directly moving the sampling points of the channel, which may lead to unrealistic river trajectories.

a scalar field  $c : \mathbb{R}^2 \rightarrow \mathbb{R}$ , which can be interactively modified by the user using classical brush tools. We directly influence the migration direction by computing the gradient  $\nabla c(\mathbf{p})$  of this scalar field. By using radial functions, we easily define attraction (where  $c(\mathbf{p}) > 0$ ) and repulsive (where  $c(\mathbf{p}) < 0$ ) constraints. In our method, we modify Equation 1 from geomorphology to incorporate the control field gradient direction as:

$$\mathbf{p}_k(t + \delta t) = \mathbf{p}_k(t) + \mu(\mathbf{p}_k(t)) (\mathbf{n}_k(t) + \nabla c(\mathbf{p})) \delta t \quad (7)$$

Figure 14 shows the influence of attractive and repulsive regions on the simulation. While negative areas are intuitive to control, we found that attraction regions more difficult to manipulate as they tend to over-constrain the simulation, leading to unrealistic trajectories.

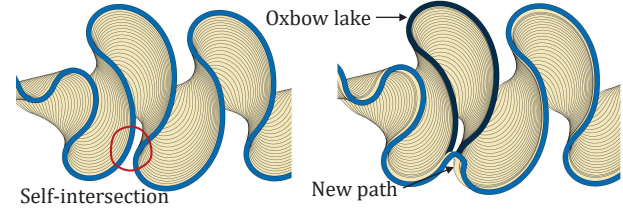


Fig. 16. Oxbow lakes automatically form where a meander starts to self-intersect, leading to an abandoned channel.

## 5 EVENTS

The dynamic of meandering rivers does not only depend on the migration of the channel but also catastrophe events. In particular, *cutoffs* are a crucial process and occur frequently during migration (Section 5.1). Additionally, the presence of *crevasses* and later the triggering of *avulsions* (Section 5.2) play a critical part in the generation of meandering trajectories. Our approach simulates those processes either using a stochastic approach or according to authoring controls.

### 5.1 Cutoffs

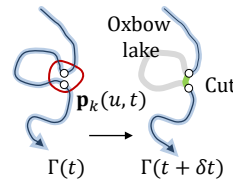


Fig. 15. Cutoff event leading to the formation of an oxbow lake.

Cutoffs occur when the channel starts to intersect itself. The channel abandons its current trajectory, which becomes an *oxbow lake* and continues onto the shorter path (see Figure 15). The oxbow lake can remain partially filled with water or dry out depending on environmental conditions. Vegetation may grow in these locations due to the water stored in the ground. Cutoff events are a fundamental process of meandering rivers as they regulate the formation of

bends.

During the simulation, we trigger a cutoff event when the distance between two (non consecutive) points within a channel is inferior to the channel width  $w_\Gamma$  [Howard and Knutson 1984]:

$$\exists (i, j) \in [0, n - 1]^2 \mid \|\mathbf{p}_i(t) - \mathbf{p}_j(t)\| \leq w_\Gamma$$

We insert a new segment between  $\mathbf{p}_i$  and  $\mathbf{p}_j$ , and the abandoned part is removed from the channel and saved in the recorded data  $\mathcal{D} = \{\mathcal{N}(t)\}$ . Figure 16 illustrates the cutoff process.

A fundamental aspect of oxbow lakes is their influence on the surrounding landscape. Figure 17 displays the recording of oxbow lakes through a simulation over hundreds of years. The channel belt, characterized as the terrain region covered by previous channel trajectories, depends on the river width and terrain topography. Section 8 details the computation of the vegetation density and the sediment layers from the recorded data of oxbow lakes.

### 5.2 Crevasses and avulsions

Crevasses randomly occur when the water flow exceeds the channel capacity, breaks the levee, and generates large sediment lobes

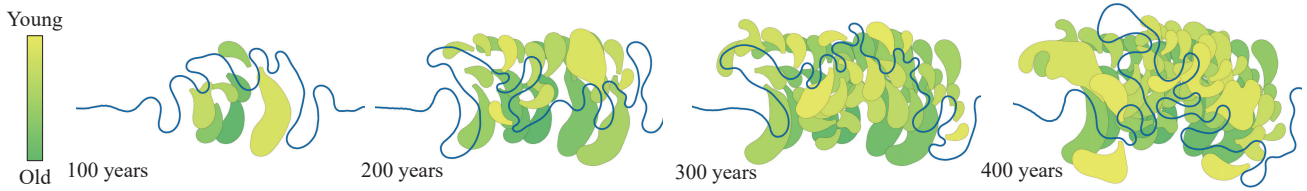


Fig. 17. Recording of all oxbow lakes through the simulation, shaded from oldest (green) to youngest (yellow). The union of all ancient trajectories form the meander belt.

that are fluvial sediment deposited in the floodplain. They usually occur at high curvature spots along the channel (Figure 18, left), but the exact formation process remains an active area of research in Geomorphology. We model crevasses stochastically as follows: at every step, we select channel points  $p_k(t)$  with a curvature  $\phi$  above a given user-defined threshold  $t_c = 0.1$ , and trigger the formation of a crevasse based on a probability  $\rho_c = 0.05$ .

Avulsions occur at the location of crevasses. As for crevasses, their exact activation conditions remain an active research topic in Geomorphology and may be related to intense rainfall causing a sudden overflow in the channel.

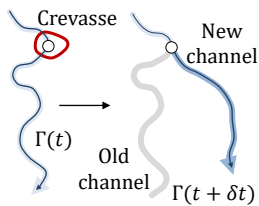


Fig. 18. Avulsion process in a channel.

The upstream part of the channel remains unchanged whereas the downstream part is abandoned and replaced by a completely new path, starting at the location of the crevasse (see Figure 18, right). Simulating avulsion requires defining a hydrologically consistent trajectory compatible with the terrain topography and collision detection with the set of channels of the network, which may be computationally intensive.

Motivated by the interactivity required by an authoring approach, we simulate local avulsions that connect a crevasse with another point downstream within the same channel and let aside paths that may connect to other channels in the network (see Section 8.5 for a discussion). For every crevasse located at a point  $a$  in a channel  $\Gamma$ , an avulsion may occur with a probability  $\rho_a$  at each simulation step. We select the endpoint of the avulsion  $b$  at a random distance within the channel  $\Gamma$  at a downstream location. The initial avulsion direction  $d$  is first computed randomly in the direction of the tangent  $t(a)$  with an opening angle  $\alpha$  randomly selected in  $[0, \alpha_0]$ , with  $\alpha_0$  set to 45 degrees in our implementation (see Figure 19). The new path  $\tilde{\Gamma}$  connecting  $a$  to  $b$  is then computed iteratively by performing a random walk from  $a$  towards  $b$  using the channel sampling distance as a stepping distance. To ensure that the path converges to the endpoint  $b$  of the avulsion, we adapt the walking direction at every step. Let  $\hat{u}$  denotes the unit straight-line avulsion direction  $\hat{u} = (b - a) / \|b - a\|$ .

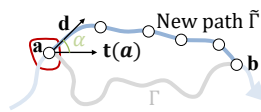


Fig. 19. Procedurally generated avulsion path.

The next direction for a point  $p$  along the avulsion path is computed as  $d(p) = t \hat{u} + (1 - t) d$  with  $t = \|p - b\| / \|a - b\|$ . Therefore, the stepping direction progressively changes so that stepping progressively converges to the  $b$ . We finally displace the direction by a small random angle in  $[-5, 5]$  degrees to avoid unnatural smooth paths.

Figure 20 shows the development of an avulsion on a single channel, leading to the formation of a new path  $\tilde{\Gamma}$  and an abandoned trajectory. While this technique is computationally efficient and authorizes some form of trajectory control through the angle  $\alpha$ , the path  $\tilde{\Gamma}$  may not be hydrologically consistent as there is no guarantee that it follows the steepest slope of the underlying terrain.

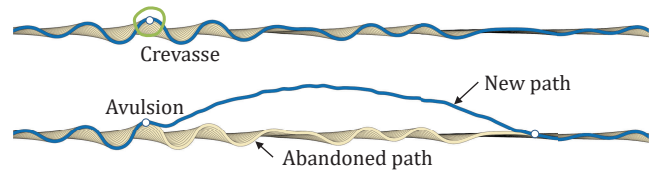


Fig. 20. During an avulsion event, the crevasse becomes the starting point of a new channel.

To solve this problem, we locally change the elevation  $h$  of terrain along the path of the new channel. For every point  $p_k$  in the new  $\tilde{\Gamma}$ , we compute the slope in the direction of the tangent  $t_k$ . If  $0 < s_t(p_k) < \epsilon_a$ , we carve the terrain to preserve a hydrologically consistent network; otherwise the slope is incompatible with the flow (and would require significant carving) and we abort the avulsion completely.

Because meandering rivers materialize in plains, the terrain slope remains small. Therefore, it is generally possible to breach the terrain with a limited amount of removed material and successfully synthesize a hydrologically-consistent channel. More accurate strategies would be possible yet at the expense of a more computationally intensive algorithm preventing interactive feedback (see Section 8.5).

## 6 NETWORK SIMULATION

The previous section describes the meandering river simulation of a single river channel. In this section, we extend the simulation to an evolving river network  $\mathcal{N}(t)$  whose set of channels  $\{\Gamma_i\}$ ,  $i \in [0, n[$  are migrating. We first describe junctions between channels and the graph structure of the river network (Section 6.1), and then address collision events that occur during the simulation and require updating the graph structure.

## 6.1 Junction models

Recall that junctions are geometric nodes  $\mathbf{q}_{ijk}$  in the graph  $\mathcal{N}$  connecting two upstream rivers  $\Gamma_i$  and  $\Gamma_j$  into a downstream river  $\Gamma_k$  (Section 3.1).

Simulating the evolution of junctions is a challenging topic of research and results from different physical processes [Guillén-Ludeña et al. 2016]. Therefore, junctions remain static during the simulation. Our model takes inspiration from the observation made in Geomorphology that the connection angle between two channels depends on their respective flows. When the junction involves two channels with significantly different water flows (thus, different widths  $w_{\Gamma_i}$  and  $w_{\Gamma_j}$ ), the connection is almost orthogonal, while two channels of similar flows usually lead to a narrow connection angle junction [Hooshyar et al. 2017] (see Figure 21).

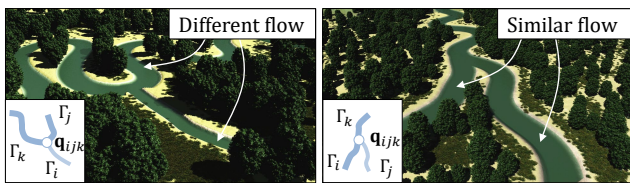


Fig. 21. We define procedural junction templates for modeling channels intersections (shown as insets), with a near perpendicular angle for rivers with different flow values (left), and a small angle for channels with similar flow values (right).

We propose the following procedural approach for handling junctions. The migration is progressively attenuated near both ends of the channels to avoid displacing junction points during the simulation (Section 4.1). This constraint allows us to procedurally place channel junction templates based on the flows of the respective channels (see Figure 21). The templates are parameterized and can be tuned by the user in a post-processing step.

## 6.2 Collision between sections

Junction templates and the migration falloff applied to the channel ends prevent collisions in the vicinity of junctions. Still, collisions between different channels may occur when the lateral migration rate is as high as several meters a year. This is solved by performing topological operations on the underlying graph of the network. We identify three cases: upstream collision, downstream collision, and collisions between disconnected channels (Figure 22).

*Upstream and downstream collisions* involve three connected channels  $\Gamma_i$ ,  $\Gamma_j$ ,  $\Gamma_k$  connected at a junction point  $\mathbf{q}_{ijk}$ . For this type of collision, we define a new junction point  $\tilde{\mathbf{q}}_{ijk}$  at the intersection point between  $\Gamma_i$  and  $\Gamma_j$  (upstream or downstream, respectively), and the downstream section of channel  $\Gamma_j$  is abandoned (see Figure 22, left and center). Those two cases neither require the creation of a new channel nor a redirection of the flow.

If a collisions between *disconnected channels* in the network  $\Gamma_i$  and  $\Gamma_j$  occur, we first change the network topology and the update the characteristics of the channels. a new junction point  $\tilde{\mathbf{q}}_{ijk}$  is created at the intersection point. If the flow of channel  $\Gamma_i$  (respectively  $\Gamma_j$ ) is greater than the flow of channel  $\Gamma_j$  (respectively  $\Gamma_i$ ), we create

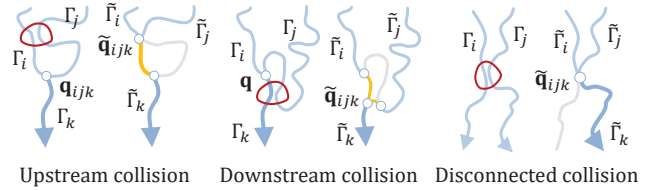


Fig. 22. Three different cases arising in collision detection.

a new channel  $\Gamma_k$  with the trajectory of the downstream part of the channel  $\Gamma_i$  (respectively  $\Gamma_j$ ), and remove the remaining part of the other channel from the network. Finally, we update the channel characteristics by recomputing their characteristics (such as flow, width, and depth), which affect the migration process, and therefore the channel sinuosity.

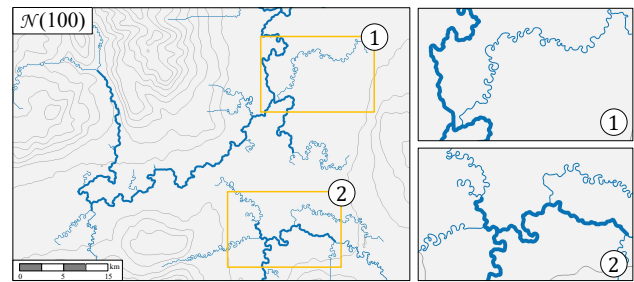


Fig. 23. Generalizing the channel simulation to an entire river network allows generating complex terrains. In plains, meandering patterns arise, while channels on steep slopes remains straight and follow the gradient of the terrain.

Figure 23 shows the result of the network simulation on a  $35 \times 35$  km terrain with multiple channels. Junctions remained static throughout the simulation.

## 7 GENERATION FROM RECORDED DATA

As meandering rivers develop rapidly, they have a powerful impact on the surrounding ecosystem. Reproducing the complex dynamics between ecosystems and meanders would involve a computationally intensive combined simulation of the two phenomena, which remains a challenging area of research in Geosciences [Ielpi et al. 2022].

Simulating the evolution of the river network through time provides us with information embedded in the description of the previous river trajectories (river paths, oxbow lakes) for all simulation steps in the recorded set of networks  $\{\mathcal{N}(t)\}$ . Therefore, we exploit these data to procedurally generate sediment deposition and compute abiotic parameters (Figure 25) which are needed for generating the vegetation density within the river belt and the bedrock covered with sediment.

We compute soil moisture from the simulation recorded data  $\mathcal{D} = \{\mathcal{N}(t)\}$  as a scalar field  $m : \mathbb{R}^2 \rightarrow \mathbb{R}$ , defined as the combination between the stream power field  $p : \mathbb{R}^2 \rightarrow \mathbb{R}$  [Cordonnier et al. 2016]

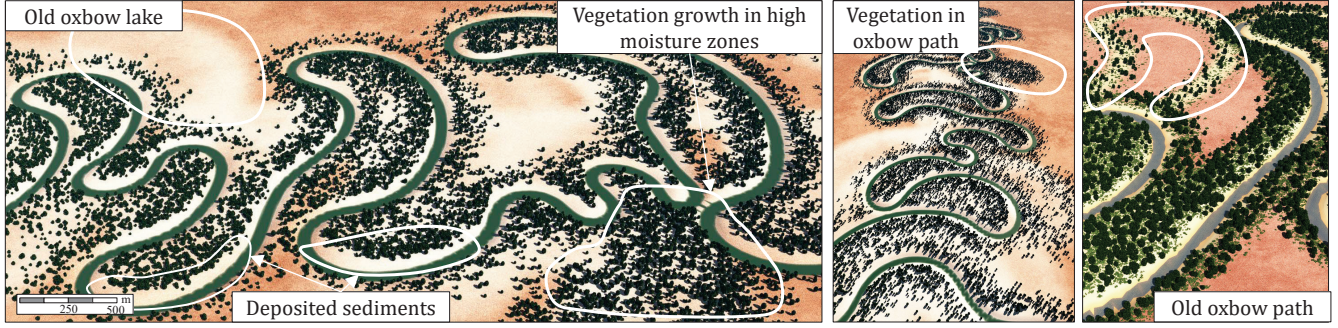


Fig. 24. Computing abiotic parameters such as soil moisture and sediment deposition allows for complex landscape modeling with visible old channel paths and oxbow lakes, and vegetation developing within the belt of the different channels.

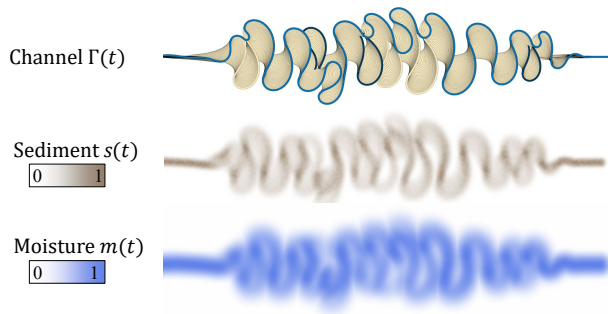


Fig. 25. Moisture and sediment deposition maps computed from the recorded simulation data  $\mathcal{D} = \{\mathcal{N}(t)\}$ .

and the sum of past moisture fields  $m_i : \mathbb{R}^2 \rightarrow \mathbb{R}$ :

$$m(\mathbf{p}) = p(\mathbf{p}) + \sum_{i=0}^n m_i(\mathbf{p}), \quad m_i(\mathbf{p}) = \varepsilon_m (g_M \circ d(\mathbf{p}, \mathcal{N}_i)) \quad (8)$$

The parameters  $\varepsilon_m \in [0, 1]$  represents the moisture accumulated at every step. A high number of simulation steps  $n$  accounts for older trajectories, whereas  $n = 1$  considers the latest network  $\mathcal{N}(t)$  only. The falloff function  $g_M$  weights the influence of the channels according to the distance to the nearest channel of the network  $d(\mathbf{p}, \mathcal{N}_i)$  and a radius of influence  $r_m$  (Figure 26).

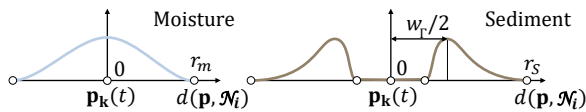


Fig. 26. Moisture  $g_M$  and sediment  $g_S$  profile curves.

The computation of the accumulation of sediment is approximated similarly. At every step, we compute sediment deposition along the channel trajectories as follows:

$$s(\mathbf{p}) = \sum_{i=0}^n s_i(\mathbf{p}), \quad s_i(\mathbf{p}) = \varepsilon_s (g_S \circ d(\mathbf{p}, \mathcal{N}_i)) \quad (9)$$

The profile curve of the falloff function  $g_S$  is parameterized by the width of the channel (see Figure 26) and a radius of influence  $r_s$ . The parameter  $\varepsilon_s \in [0, 1]$  denotes the accumulated sediment quantity in meters for each simulation step.

Figure 24 shows the effect of accumulated sediments located on ancient oxbow lakes and along the past channel trajectories. Combined with soil moisture, we also generate the vegetation density from the recorded data, with dense vegetated areas emerging within the river belt and close to old channels and oxbow lakes. These procedural and controllable approximations are used to efficiently augment the terrain with vegetation and sediments, without resorting to an otherwise complex simulation that would not allow interactive editing.

## 8 RESULTS AND DISCUSSION

We implemented our method in C++. Experiments were performed on a desktop computer equipped with Intel® Core i7, clocked at 4 GHz with 16 GB of RAM, and an NVIDIA GTX 1080ti graphics card. The output was directly streamed into E-On Software VUE® to produce photo realistic landscapes (Figure 21, 24, 27, 28). The source code for reproducing the results is available at <https://github.com/aparis69/Meandering-rivers>.

### 8.1 Control and authoring

All the images in the article were authored in real-time and demonstrate the authoring capacities of our method. Figure 29 illustrates characteristic consecutive steps in an interactive editing session. Starting from an initial low-resolution river network  $\mathcal{N}(0)$ , the designer let the simulation initiate the meandering process. She raised hills and mountains around a specific channel, constraining its path, before introducing repulsive constraints to gradually guide the migration process toward the center of the landscape. She finally modified the network by extending a mountain range, which deleted a meandering channel, and added a new channel.

Figure 27 shows a three-stage meandering complex. In plains, the channel migrates freely and meanders as well as oxbow lakes develop. Steep slopes cancel the migration term and therefore produce straight river trajectories in the transition zone. In valleys surrounded by mountains, the channel exhibits constrained meandering patterns that sometimes stabilize during the simulation.

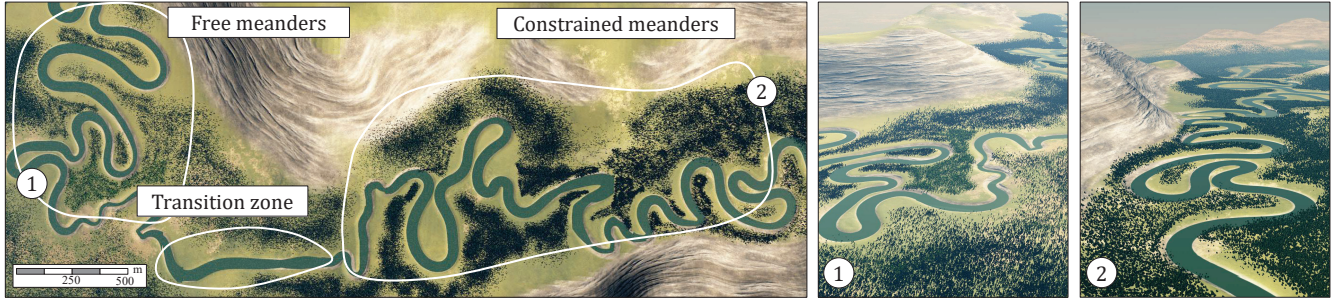


Fig. 27. Result of the simulation where the channel is constrained by the surrounding mountains (right) and free in plains (left).

Controlling physically-based simulations may be challenging, particularly in the case of highly dynamic systems such as meandering rivers. Nonetheless, our model bridges the gap between authoring and simulation. First, the vector-based curve representation of rivers is efficient and allows real-time feedback even with landscapes featuring hundreds of channels. Second, the migration equation includes terms that allow control at *channel* and *network* scale.

At *channel* scale, the user may adjust the parameters of the simulation such as the width and depth of the channels (Section 4). She may modify the relief of the terrain at any time and let the simulation adapt (Section 4.4). Attraction and repulsion regions are particularly adapted to precisely locate meandering zones in the landscape while preserving the overall consistency of the physically-based approach (Section 4.5). In our implementation, the system automatically triggers avulsions in a stochastic way according to a probability prescribed by the user (Section 5.2). Alternatively, the user may also activate such events manually.

At *network* scale, the designer may modify the nodes or the trajectories of the underlying graph, create or remove channels, or directly change their trajectories (see accompanying video) while the simulation runs. We handle junctions between multiple channels using procedural patterns based on archetypes identified in Geomorphology (Section 4.5). Even though our framework currently implements two types of junctions, it can be easily complemented with other template models.

Landscape artists need tools to automate the creation of plausible river trajectories over large terrains while guaranteeing control. We submitted our work to professional landscape artists working in the entertainment industry. They confirmed the need for interactive techniques for authoring river trajectories and controlling the meandering processes. In particular, the ability to naturally enhance the river trajectories while respecting the terrain constraints was identified as a crucial feature; our approach to bridging the gap between simulation and control is a step forward in this direction. Note that artists mentioned the need for authoring braided rivers and deltas, which is a promising avenue for future research.

## 8.2 Performance

Table 2 reports the statistics for different scenes shown throughout this paper. Timings show that the simulation runs in real-time for networks of moderate size (number of sampling points  $\#\Gamma \lesssim 5\,000$ ),

and at interactive rates even for large networks featuring hundreds of river channels.

Figure	Domain		Simulation			
	Size	$\#\Gamma$	Steps	$\#C$	$t_s$ (ms)	$t_c$ (s)
10	$16 \times 25$	2 521	350	54	7.6	2.7
11	$10 \times 10$	403	130	1	0.6	0.8
14	$10 \times 10$	323	160	2	0.6	1.0
27	$35 \times 20$	1 571	1 134	530	12.5	14.2
29	$35 \times 35$	9 807	1 400	5 132	36.2	51.6

Table 2. Statistics for different scenes: size (in  $\text{km} \times \text{km}$ ), number of sampling points  $\#\Gamma$ , simulation steps, number of cutoff events  $\#C$ , time for single step  $t_s$  (ms), and total simulation time  $t_c$  (s).

In our experiments, processing time grows linearly with respect to the number of sampling points  $\#\Gamma$  and the number of cutoff events  $\#C$ . Figure 29 illustrates the most computationally intensive case with  $\approx 10\,000$  sampling points processed at each simulation step, and  $\approx 5\,000$  cutoff events.

## 8.3 Validation

As rivers are an active research subject in Geomorphology and, more broadly, in Geosciences, different metrics exist to describe, compare, and quantify meandering rivers. While we do not aim at an exhaustive comparison, we implemented several metrics and compare the obtained values against real data. Particularly, we focus on the meander wavelength and sinuosity of the channels (Table 3).

Meander wavelength  $\lambda$  is defined as the spacing between two consecutive inflection points in the channel [Reinfelds and Bishop 1998]. Various authors have studied the relationship between meander wavelength and river width and all end up with a power law relation of the form  $\lambda = a w_\Gamma^b$  with  $6.28 \leq a \leq 12.34$ , and  $[1 \leq b \leq 1.13]$  [Leopold and Wolman 1960; Yalin 1972]. Williams [1986] provides the associated error estimations, which indicate that values for  $\lambda$  can be expected to fall within about  $-40\%$  to  $+65\%$  of the estimated value. With that in mind, one can estimate realistic wavelengths to be comprised between  $[314, 990]$  m for  $w_\Gamma = 50$  m,  $[628, 2150]$  for  $w_\Gamma = 100$  m, and  $[1256, 4674]$  for  $w_\Gamma = 200$  m. All the generated networks show acceptable values as compared to real systems (Table 3).

Figures	Width $w_r$	Wavelength $\lambda$	Sinuosity $\sigma$
10	[50, 200]	[710, 1680]	[1.9, 3.8]
11	200	2160	2.4
14	200	1840	1.9
27	200	1600	3.1
Observed	Any	[314, 4674]	> 1.5

Table 3. Geomorphological properties of different scenes: river width  $w_r$  in meters, meander wavelength  $\lambda$  in meters, and sinuosity  $\sigma$ . The last line reports the range of values measured for real rivers: intervals for the wavelength have been computed using formula and associated standard deviation found in literature for the considered channel width.

We also analyzed our results with respect to channel sinuosity metric. Recall that the sinuosity  $\sigma$  is defined as the ratio between the curvilinear length of the curve and the distance between the first and last points of the channel (Equation 3). Standard classifications state that the meandering stage of a river starts at  $\sigma > 1.5$ . Our results consistently conform to observations in Geomorphology as reported in Table 3.

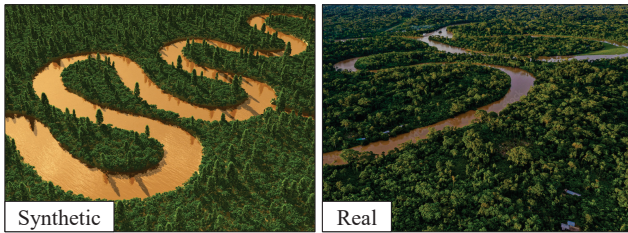


Fig. 28. Visual comparison of a synthesized meandering river in a rain forest and a real image (from Adobe stock.)

Finally, we provide a visual comparison of a synthetic river against a photograph (Figure 28). In this scene, the user manually created an initially straight channel, and ran a 100-steps simulation, before adding vegetation. This demonstrates that our method can reproduce various bend patterns commonly observed in real rivers.

#### 8.4 Comparison with other methods

Our method compares favorably to previously published work in Computer Graphics. Procedural approaches for modeling river networks [Génevaux et al. 2013; Peytavie et al. 2019] synthesize static channels and do not simulate their evolution throughout time. Therefore, they do not capture the complex time-evolving patterns arising from a multi-factorial migration process. Moreover, while those approaches based on Rosgen classification [Rosgen 1994] reproduce different types of rivers such as braided rivers or mountain creeks, they define river trajectories and riverbed profiles procedurally as a collection of static spline-based template primitives stored in an atlas. This approach lacks information to generate sediment along past trajectories as well as moisture data for adding a vegetation cover to the terrain (Section 7) because of the fixed models stored in the atlas of river segments.

Surface erosion algorithms based either on particles [Křištof et al. 2009; Skorkovská et al. 2019] or shallow water simulations are computationally intensive, do not provide direct control, and require a fine-tuning of the initial conditions to reproduce interesting meandering patterns. In contrast, the curve-based model provides both physical accuracy and allows for interactive feedback during authoring.

Based on the algorithm proposed by [Sylvester et al. 2019], our method naturally inherits from the hydraulic rules proposed by [Howard and Knutson 1984; Ikeda et al. 1981] and from the empirical observations made by various geomorphologists (such as the relations between width and depth, and between the local migration rate, the width, and the curvature). In contrast, we account from contextual parameters like topography, and upstream migration rates, which is not the case for geostatistical approaches.

For authoring and efficiency purpose, and as we aim here at modeling landscapes and not a plurimetric sedimentary record as geoscientists do, our approach is simplest than the physical-based one initiated by [Lopez 2003; Lopez et al. 2009] in the Flumy software: we do not integrate the long-term vertical aggradation, the levee breaches and crevasse splay generations, and the rock type diversity that they manage. However, we model river networks, *i.e.* ensembles of connected channels, while models from the geoscientific community only deal with one single, possibly migrating river or several independent channels stacked in a sedimentary pile.

Concerning the interactivity, our approach uses topography as a way to indirectly control the river trajectory, in an intermediate way between the repulsive and attractive vectors proposed by [Rongier et al. 2017b] in L-system channel modeling and the topography modification used in Flumy [Anna Bubnova 2018]. Contrary to both of these methods designed to well honor data, here we aim a smooth interactive control during the simulation.

#### 8.5 Limitations

Our method simulates synthetic meandering rivers with properties comparable to real ones. However, it does not come without limitations. First, our model is based on a 2D physically-based simulation [Sylvester et al. 2019] that models a merely regular downstream migration of the channel centerline. The mapping of this model on the 3D terrain may produce riverbed geometries slightly flowing upward, which sometimes occurs in real rivers. Like in all realizations based on [Ikeda et al. 1981] equations, the resulting meander geometries seem to be slightly distorted oppositely to the flow direction. This is mainly visible when the simulation is run from an initial nearly linear initial trajectory on a flat topography (*e.g.*, Figure 11, 16). The carving process may be easily modified to guarantee that the river flows downward along the entire trajectory.

Other studies, *e.g.* on Mississippi [Parquer et al. 2017], have demonstrated that lateral migration show much more diversity than what has been modeled in [Sylvester et al. 2019], and that uncoupling lateral migration into tangential and normal offsets could improve realism and increase the range of patterns that can be created. If such decomposition would potentially slow down the simulation process, the geostatistical approaches proposed by [Rongier et al.

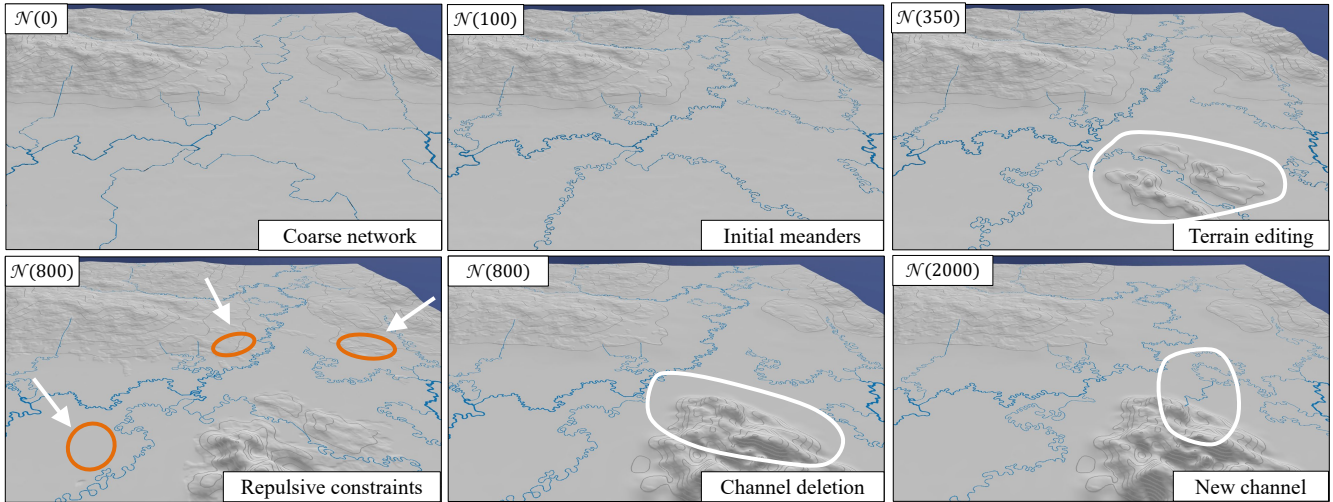


Fig. 29. Overview of a typical authoring session: starting from a low-resolution river network  $\mathcal{N}(0)$ , the user freely modifies the relief, introduces repulsion regions and even adds new rivers: the simulation automatically computes the evolving network  $\mathcal{N}(t)$  according to the designer’s prescriptions.

2017a] would be worth investigating, at least to compare with the physically-based approaches.

Second, the current models for channel does not really integrate the observed asymmetry of the erosion (on the outer bank) and deposition (on the inner bank) which constitute the sandy deposits of the accretion bars: sandy banks should be more visible on the inner banks, gradually colonized by vegetation, while the outer banks should be more abrupt, with a sharper transition from river to vegetation. For efficiency purpose, a symmetric sediment deposition profile curve is used to model levees, which permits to approximate the inner bank deposition as demonstrated in Figure 25.

Third, we do not model the mutual feedback between vegetation and the development of the river, which is still an active area of research in Geosciences [Ielpi et al. 2022]. Instead, we rely on an efficient procedural approach for computing abiotic parameters such as soil moisture and sediment deposition (Section 7), which are then used as input parameters to generate vegetation density interactively.

Also in details, abandoned meanders are generally filled by shales, while accretion bars are made of sands. Integrating these particularities could be a way to differentiate the vegetation in the landscape, as shales and sands have quite opposite permeability, porosity, and mineralogical composition, all factors strongly impacting the species that would develop. These approximations are a typical tradeoff between interactivity and accuracy.

Finally, we model channels with a constant width  $w_{\Gamma}$  and depth  $d_{\Gamma}$ . Although standard an approximation in Geosciences [Sylvester et al. 2019], this strategy does not account for probable variations along the channel path. This restriction is partially alleviated by the interactivity of our system and control tools: the user may split a channel into two distinct ones and adapt their characteristics as desired. In the same spirit, we only simulate *local* avulsion within a given channel (Section 5.2). A more complicated, therefore computationally intensive, algorithm could generate more complex paths

between different channels and properly recompute the flow and, consequently, change the river parameters. Previous methods in Geosciences rely on an L-system for computing the new path of the channel [Rongier et al. 2017a] but do not lend themselves to a complex river network. A possible solution would compute the anisotropic shortest path between the avulsion point and a randomly selected point in the downstream river network, accounting for the slope and the existing channels to avoid unwanted collisions.

## 9 CONCLUSION

We introduced a method for modeling meandering river networks at the interface between interactive authoring and accurate simulation. Inspired by physically-based models proposed in Geomorphology, we augmented the global migration equation with extra terms and parameters to account for topography characteristics and user constraints, allowing for efficient user control. The proposed migration model inherits from the impact of the local and upstream curvature and reproduces patterns and landforms observed in rivers such as bend migration, oxbow lake formation, and changes of trajectory due to avulsion. We extend the simulation to a complete river network encoded as a directed graph and show how to solve collisions and procedurally handle junction points between channels. The user may control the simulation directly by interacting with the river control points, or indirectly through control regions that influence the migration of the different channels. Our method conforms to observations in Geomorphology concerning statistical measures of the channel trajectories.

This work unlocks several avenues for future research. A direct extension would be to model the two-way coupling between ecosystem and meander simulation in the spirit of the interleaved simulation introduced in [Cordonnier et al. 2017]. Simulating and authoring other macroscale landforms such as braided rivers and deltas examined in Geomorphology [Murray and Paola 1997; Thomas and

Nicholas 2002], and more generally coastlines, is another direction particularly worth investigating.

## ACKNOWLEDGMENTS

This work was part of the project AMPLI ANR-20-CE23-0001 and EOLE ANR, supported by Agence Nationale de la Recherche Française.

## REFERENCES

- Anna Bubnova. 2018. *On the conditioning of process-based channelized meandering reservoir models on well data*. Ph.D. Dissertation. Paris Sciences et Lettres - Mines ParisTech.
- Richard Barnes, Clarence Lehman, and David Mulla. 2014. Priority-flood: An Optimal Depression-filling and Watershed-labeling Algorithm for Digital Elevation Models. *Computers & Geosciences* 62 (2014), 117–127.
- Farès Belhadj and Pierre Audibert. 2005. Modeling Landscapes with Ridges and Rivers: Bottom Up Approach. In *Proc. International Conference on Computer Graphics and Interactive Techniques in Australasia and South East Asia*. ACM, 447–450.
- Bedřich Beneš, Václav Těšínský, Jan Hornýš, and Sanjiv K. Bhatia. 2006. Hydraulic erosion. *Computer Animation and Virtual Worlds* 17, 2 (2006), 99–108.
- Antoine Bertoncello, Tao Sun, Hongmei Li, Gregoire Mariethoz, and Jef Caers. 2013. Conditioning Surface-Based Geological Models to Well and Thickness Data. *Mathematical Geosciences* 45, 7 (2013), 873–893.
- E. Black, C.E. Renshaw, F.J. Magilligan, J.M. Kaste, W.B. Dade, and J.D. Landis. 2010. Determining lateral migration rates of meandering rivers using fallout radionuclides. *Geomorphology* 123, 3 (2010), 364–369.
- Rocko A. Brown and Gregory B. Pasternack. 2019. How to build a digital river. *Earth Science Reviews* 194 (2019), 283–305.
- Rolf Clemetsen, AR Hurst, Ragnar Knarud, and Henning Omre. 1990. A computer program for evaluation of fluvial reservoirs. In *North Sea Oil and Gas Reservoirs—II*. Springer, Springer Netherlands, Dordrecht, 373–385.
- Guillaume Cordonnier, Jean Braun, Marie-Paule Cani, Bedřich Beneš, Éric Galin, Adrien Peytavie, and Éric Guérin. 2016. Large Scale Terrain Generation from Tectonic Uplift and Fluvial Erosion. *Computer Graphics Forum* 35, 2 (2016), 165–175.
- Guillaume Cordonnier, Eric Galin, James Gain, Bedřich Beneš, Eric Guérin, Adrien Peytavie, and Marie-Paule Cani. 2017. Authoring Landscapes by Combining Ecosystem and Terrain Erosion Simulation. *ACM Transactions on Graphics* 36, 4 (2017), 12.
- Clayton Deutsch and Toan Thai Tran. 2002. FLUVSIM: a program for object-based stochastic modeling of fluvial depositional systems. *Computers & Geosciences* 28, 4 (2002), 525–535.
- Clayton Deutsch and Libing Wang. 1996. Hierarchical object-based stochastic modeling of fluvial reservoirs. *Mathematical Geology* 28, 7 (1996), 857–880.
- Thomas Dunne. 1978. Field studies of hillslope flow processes. *Hillslope hydrology* (1978), 389–227.
- Eric Galin, Eric Guérin, Adrien Peytavie, Guillaume Cordonnier, Marie-Paule Cani, Bedřich Beneš, and James Gain. 2019. A Review of Digital Terrain Modeling. *Computer Graphics Forum (proceedings of Eurographics 2019 STAR)* 38, 2 (2019), 553–577.
- Jean-David Gènevaux, Éric Galin, Éric Guérin, Adrien Peytavie, and Bedřich Beneš. 2013. Terrain Generation Using Procedural Models Based on Hydrology. *ACM Transaction on Graphics* 32, 4 (2013), 143:1–143:13.
- Eric Guérin, Adrien Peytavie, Simon Masnou, Julie Digne, Basile Sauvage, James Gain, and Eric Galin. 2022. Gradient Terrain Authoring. *Computer Graphics Forum* 41, 2 (2022), 85–95.
- Sebastián Guillén-Ludeña, Mário J. Franca, Antonio Cardoso, and A. J. Schleiss. 2016. Evolution of the hydromorphodynamics of mountain river confluences for varying discharge ratios and junction angles. *Geomorphology* 255 (2016), 1–15.
- Houssam Hnaidi, Éric Guérin, Samir Akkouché, Adrien Peytavie, and Éric Galin. 2010. Feature based terrain generation using diffusion equation. *Computer Graphics Forum* 29, 7 (2010), 2179–2186.
- Milad Hooshyar, Arvind Singh, and Dingbao Wang. 2017. Hydrologic controls on junction angle of river networks. *Water Resources Research* 53, 5 (2017), 4073–4083.
- Alan Howard and Thomas Knutson. 1984. Sufficient Conditions for River Meandering: A Simulation Approach. *Water Resources Research* 20 (11 1984), 1659–1667.
- Richard J. Huggett. 2003. *Fundamentals of Geomorphology*. Routledge.
- Alessandro Ielpi, Mathieu Lapôte, C. Boyce, and Martin Gibling. 2022. The impact of vegetation on meandering rivers. *Nature Reviews Earth & Environment* 3 (2022), 1–14.
- Syunsuke Ikeda, Gary Parker, and Kenji Sawai. 1981. Bend theory of river meanders. Part 1. Linear development. *Journal of Fluid Mechanics* 112 (1981), 363–377.
- Alex D. Kelley, Michael C. Malin, and Gregory M. Nielson. 1988. Terrain simulation using a model of stream erosion. *Computer Graphics* 22, 4 (1988), 263–268.
- Kory Konsoer, Jessica Zinger, and Gary Parker. 2013. Bankfull hydraulic geometry of submarine channels created by turbidity currents: Relations between bankfull channel characteristics and formative flow discharge. *Journal of Geophysical Research: Earth Surface* 118, 1 (2013), 216–228.
- Peter Křištof, Bedřich Beneš, Jaroslav Krivánek, and Ondřej Šťava. 2009. Hydraulic Erosion Using Smoothed Particle Hydrodynamics. *Computer Graphics Forum* 28, 2 (2009), 219–228.
- Michał Kurowski. 2012. Procedural generation of meandering rivers inspired by erosion. *WSCG'2012*.
- Luna B. Leopold and M. Gordon Wolman. 1960. River Meanders. *GSA Bulletin* 71, 6 (1960), 769–793.
- Simon Lopez. 2003. *Modélisation de réservoirs chenalisés méandriformes: approche génétique et stochastique*. Ph.D. Dissertation. Ecole des Mines de Paris.
- Simon Lopez, Isabelle Cojan, Jacques Rivoirard, and Alain Galli. 2009. Process-Based Stochastic Modelling: Meandering Channelized Reservoirs. *Analog. Numer. Model. Sediment. Syst. From Underst. to Predict.* (2009), 139–144.
- Bart Makaske. 2001. Anastomosing rivers: a review of their classification, origin and sedimentary products. *Earth-Science Rev.* 53, 3-4 (2001), 149–196.
- A. Brad Murray and Chris Paola. 1997. Properties of a cellular braided-stream model. *Earth Surface Processes and Landforms* 22, 11 (1997), 1001–1025.
- Takeshi Nakajima, Jeffrey Peakall, William McCaffrey, Douglas Paton, and Philip Thompson. 2009. Outer-Bank Bars: A New Intra-Channel Architectural Element within Sinuous Submarine Slope Channels. *Journal of Sedimentary Research* 79 (2009), 872–886.
- Marion N. Parquer, Pauline Collon, and Guillaume Caumon. 2017. Reconstruction of Channelized Systems Through a Conditioned Reverse Migration Method. *Mathematical Geosciences* 49, 8 (2017), 965–994.
- Adrien Peytavie, Thibault Dupont, Eric Guérin, Yann Cortial, Benes Benes, James Gain, and Eric Galin. 2019. Procedural Riverscapes. *Computer Graphics Forum* 38, 7 (2019), 35–46.
- Henry W. Posamentier and Venkatarathnan Kolla. 2003. Seismic Geomorphology and Stratigraphy of Depositional Elements in Deep-Water Settings. *Journal of Sedimentary Research* 73, 3 (2003), 367–388.
- Przemysław Prusinkiewicz and Marc Hammel. 1993. A fractal model of mountains with rivers. In *Proceedings of Graphics Interface*. Canadian Information Processing Society, Toronto, Canada, 174–180.
- Michael J. Pyrcz, Jeff Boisvert, and Clayton Deutsch. 2009. ALLUVSIM: A program for event-based stochastic modeling of fluvial depositional systems. *Computers and Geosciences* 35, 8 (2009), 1671–1685.
- Ivars Reinholds and Paul Bishop. 1998. *Palaeohydrology and Environmental Change*. Chapter Palaeohydrology, palaeodischarges and palaeochannel dimensions: Research strategies for meandering alluvial rivers, 27–42.
- Guillaume Rongier, Pauline Collon, and Philippe Renard. 2017a. A geostatistical approach to the simulation of stacked channels. *Marine and Petroleum Geology* 82 (2017), 318–335.
- Guillaume Rongier, Pauline Collon, and Philippe Renard. 2017b. Stochastic simulation of channelized sedimentary bodies using a constrained L-system. *Comput. Geosci.* 105 (2017), 158–168.
- D. L. Rosgen. 1994. A classification of natural rivers. *Catena* 22 (1994), 169–199.
- Hugo Schott, Axel Paris, Lucie Fournier, Eric Guérin, and Eric Galin. 2023. Large-scale terrain authoring through interactive erosion simulation. *ACM Transactions on Graphics* 42, 5 (2023), 162:1–15.
- Vera Skorkovská, Ivana Kolingerová, and Petr Vaneczek. 2019. A Unified Curvature-driven Approach for Weathering and Hydraulic Erosion Simulation on Triangular Meshes. In *VISIGRAPP*. 122–133.
- R. Slingerland and Norman Smith. 2004. River avulsions and deposits. *Annual Review of Earth and Planetary Sciences* 32 (04 2004), 257–285.
- E. Stouthamer and H. J.A. Berendsen. 2001. Avulsion Frequency, Avulsion Duration, and Interavulsion Period of Holocene Channel Belts in the Rhine-Meuse Delta, The Netherlands. *Journal of Sedimentary Research* 71, 4 (2001), 589–598.
- Ondřej Šťava, Bedřich Beneš, Matthew Brisbin, and Jaroslav Krivánek. 2008. Interactive Terrain Modeling Using Hydraulic Erosion. In *Proceedings of Symposium on Computer Animation*. Eurographics Association, 201–210.
- Zoltán Sylvester, Paul Durkin, and Jacob A. Covault. 2019. High curvatures drive river meandering. *Geology* 47, 3 (02 2019), 263–266.
- R. Thomas and A.P. Nicholas. 2002. Simulation of braided river flow using a new cellular routing scheme. *Geomorphology* 43, 3 (2002), 179–195.
- Sophie Viseur, Arben Shtuka, and Jean-Laurent Laurent Mallet. 1998. New Fast, Stochastic, Boolean Simulation of Fluvial Deposits. In *SPE Annu. Tech. Conf. Exhib.* Society of Petroleum Engineers, 697–709.
- Garnett P. Williams. 1986. River meanders and channel size. *Journal of Hydrology* 88, 1 (1986), 147–164.
- MS Yalin. 1972. On the formation of dunes and meanders. in: *Hydraulic research and its impact on the environment* (1972).